Journal of Nuclear Materials 542 (2020) 152423

Contents lists available at ScienceDirect

Journal of Nuclear Materials

journal homepage: www.elsevier.com/locate/jnucmat

Spent fuel corrosion and the impact of iron corrosion – The effects of hydrogen generation and formation of iron corrosion products

A. Puranen[a,*], A. Barreiro[b], L.-Z. Evins[c], K. Spahiu[c]

[a] SVAFO AB, Nyköping, Sweden
[b] Studsvik Nuclear AB, Sweden
[c] Swedish Nuclear Fuel and Waste Management Co, Sweden

ARTICLE INFO

Article history:
Received 6 March 2020
Revised 1 June 2020
Accepted 26 July 2020
Available online 7 August 2020

ABSTRACT

Canister designs for deep geological disposal of spent nuclear fuel typically involve large amounts of iron. Canister failure will likely involve corrosion of the canister at the disposal depth several hundred meters underground, where conditions are typically anoxic. Spent nuclear fuel corrosion and dissolution will therefore likely proceed together with anoxic iron corrosion. The iron corrosion can suppress spent fuel corrosion by creation of strongly reducing conditions from Fe(II) formation and generation of large quantities of hydrogen. In an attempt to separate the effect of hydrogen from that of Fe(II) and iron corrosion products, two experiments were performed. In both cases, spent nuclear fuel powders were used in autoclaves filled with simplified granitic groundwater initially pressurized with argon. In the first experiment, the autoclave contained iron powder. Following the initial radionuclide release at start-up, the concentration of redox sensitive radionuclides decreased with uranium reaching UO_2 (am) solubility levels within months. Release of non-redox sensitive elements such as Cs ceased after 223 days. Continuous hydrogen generation was observed. XRD and Raman spectroscopy of the iron corrosion products identified magnetite. The second experiment was therefore performed starting with magnetite powder. In this case, the autoclave argon atmosphere remained constant. Radionuclide release was, however, continuous with uranium reaching $>2 \times 10^{-5}$ M after 275 days. The magnetite powder of the second experiment was analyzed and found to be composed of mainly magnetite with a small fraction of hematite. In the iron corrosion experiment, Mo, Tc and U where found to have high iron corrosion product affinities. However, in the magnetite experiment, U, Tc and Mo displayed weak affinity for the corrosion products, indicating presence in the higher oxidation state. The results thus point to hydrogen evolution being the main contributor to the apparent inhibition of radionuclide release in the iron corrosion experiment.

© 2020 The Authors. Published by Elsevier B.V.
This is an open access article under the CC BY-NC-ND license.
(http://creativecommons.org/licenses/by-nc-nd/4.0/)

1. Introduction

Concepts for deep geological disposal of spent nuclear fuel involve burial of canisters approximately 500 m underground, where conditions are expected to be anoxic. In addition, the concepts normally involve iron as a major component of the canister designs; in the KBS-3 concept, each spent fuel canister contains about 14 tons of iron inside the outer copper shell [1,2]. If a canister loses its integrity in the repository, anoxic iron corrosion is expected, potentially producing a hydrogen pressure of several MPa [3]. Hydrogen has the potential to suppress the oxidative dissolution of spent nuclear fuel [4–8]. The study of spent nuclear fuel dissolution in anoxic conditions and in the presence of corroding iron is therefore highly relevant [9–14]. Such studies are, however, scarce, at least in granitic groundwater conditions. This paper is a continuation of initial results on this topic reported in [11].

The aqueous corrosion of iron may result in several corrosion products depending on the redox conditions and the composition of the groundwater. This paper focuses on anoxic granitic groundwater conditions. In strictly reducing conditions, Fe(II)-hydroxide, ($Fe(OH)_2$), initially forms. In carbonate containing systems, the Fe(II) mineral siderite ($FeCO_3$) is a candidate [15]. In less reducing or alternating redox conditions, green rusts with Fe(II)/Fe(III) ratios of ~3–2 composed of a layered double hydroxide structure with either CO_3^{2-}, Cl^- or SO_4^{2-} anions may form [16,17]. The stability region of green rusts is, however, quite narrow. Magnetite, Fe_3O_4 (Fe(II)/Fe(III) ratio of 1/3), is, however, considered a likely major

* Corresponding author.
E-mail address: anders.puranen@svafo.se (A. Puranen).

https://doi.org/10.1016/j.jnucmat.2020.152423
0022-3115/© 2020 The Authors. Published by Elsevier B.V. This is an open access article under the CC BY-NC-ND license. (http://creativecommons.org/licenses/by-nc-nd/4.0/)

anoxic iron corrosion product [18,19], which was also observed in [9] and [20]. If the redox conditions are more oxidizing e.g. from the influx of dissolved atmospheric oxygen or oxidizing radiolysis products, Fe(III) minerals such as iron oxyhydroxides (FeOOH), or hematite/maghemite (Fe_2O_3) forms.

In the case of spent nuclear fuel corroding inside an iron canister, a redox gradient will likely develop. Reducing conditions might occur near the corroding iron surface, while radiolysis may cause more oxidizing conditions close to the fuel surface. This may lead to a complex set of interacting processes, as is outlined in [21,22]. Which of these processes dominate thus has a strong impact on the expected speciation and solubility of redox sensitive elements, such as U and Pu, and on the fuel matrix corrosion behavior.

Anoxic iron corrosion will lead to formation of dissolved Fe(II) in addition to hydrogen, both being reductants. The following section gives a brief overview of the similarities, differences and potentially synergetic interplay between Fe(II) and molecular hydrogen. Further details can be found in [22]. Dissolved Fe(II) is a one-electron reductant that is active versus all radiolytically formed oxidants (radical and molecular), and is oxidized to Fe(III), which precipitates at very low concentrations at near-neutral or higher pH. Fe(II) diffuses from the Fe-source toward the surface of the spent fuel, consuming oxidants in the path and being consumed itself. At the given temperatures, hydrogen is, on the other hand, inert toward molecular oxidants in solution and reduces only radical oxidants formed by radiolysis. In this context, H_2O_2 has been identified as a key oxidant resulting from radiolysis [22, and references within]. The concentration of hydrogen is expected to be close to constant in a stagnant solution between a corroding iron surface and near to the fuel surface because radicals are kinetically very reactive, but their concentrations in solution are extremely low compared with molecular oxidants (e.g. H_2O_2). The Fe(II) concentration might, however, decrease more sharply closer to the fuel surface because one molecule of H_2O_2 oxidizes two Fe(II) ions via the following reactions (1 and 2).

$$Fe(II) + H_2O_2 \rightarrow Fe(III) + OH^- + OH\cdot \quad (1)$$

$$Fe(II) + OH\cdot \rightarrow Fe(III) + OH^- \quad (2)$$

Hydrogen does not react directly with H_2O_2, but it can act synergistically with Fe(II) by reaction with the hydroxyl radical formed in reaction (1), resulting in atomic hydrogen (3), which is a strong reductant (see reaction 4). This can support a hydrogen-driven H_2O_2-consuming reaction chain via the hydroxyl radical and atomic hydrogen intermediaries, reactions (3, 4).

$$OH\cdot + H_2 \rightarrow H_2O + H\cdot \quad (3)$$

$$H\cdot + H_2O_2 \rightarrow H_2O + OH\cdot \quad (4)$$

Dissolved carbonate may, however, scavenge hydroxyl radicals, hindering this reaction sequence. H_2O_2 may also be catalytically decomposed into two surface adsorbed OH-radicals on surfaces such as the spent fuel doped with various amounts of fission products. It has been shown that dissolved molecular hydrogen consumes these adsorbed OH radicals [23]. The presence of noble metal inclusions (ε-particles) besides catalysing H_2O_2 decomposition [24], catalyses also dissociation of molecular hydrogen into atomic hydrogen [25], providing a strong reductant directly at the spent fuel surface.

The relative importance of these different processes varies with the conditions. In the case of a system dominated by radiolysis from α-activity, an Fe(II)-driven redox gradient was found to reach the surface of α-doped UO_2 pellets and cause apparent inhibition of the fuel matrix corrosion. Fe(III) oxidative precipitation on the UO_2 surfaces was noted, with modest hydrogen build-up (our estimation is <0.2 mM H_2 from the data given in the paper) [14]. In another study with spent fuel, which has a longer radiolysis range, due to mixed α, β and γ radiation, complete apparent inhibition of the matrix corrosion was also noted in the absence of added iron, but for a dissolved hydrogen level of 0.8 mM H_2 [7].

In this study we performed spent nuclear fuel corrosion and leaching experiments in simplified granitic groundwater under initially inert argon atmosphere conditions. The first experiment involved an autoclave with spent fuel and metallic iron powder. Part of this experiment was previously reported in [11], studying both the evolution of hydrogen, the radionuclide release and the resulting iron corrosion products. An inactive iron corrosion experiment (same conditions but no spent fuel) was also performed to study the impact of the spent fuel on the iron corrosion and hydrogen generation. Because magnetite was found to be the major corrosion product in the hydrogen generating iron corrosion cases, a third autoclave experiment was performed starting with magnetite powder instead of iron in order to separate the effects of the hydrogen generation from iron corrosion while maintaining a large surface area of Fe(II)-containing magnetite.

2. Experimental

The experiments were performed in stainless steel autoclaves (316 L alloy) that had been passivated by dilute nitric acid and thoroughly rinsed. The spent fuel (D07/S14) had been irradiated in the PWR Ringhals 2 to a local pellet average burnup of 43 MWd/kgU. Further details on the fuel can be found in [26]. A larger portion of this fuel had been crushed and sieved in a previous campaign. The mesh size fraction 0.25–0.5 mm was used in both experiments with 2 g of fuel per autoclave. Prior to start-up of the autoclave experiments, both fuels were pre-leached outside the autoclaves for a cumulative time of 8 and 13 days, respectively, to remove pre-oxidized surface layers from the crushing and storage time, as well as to remove part of the instant release fraction. The fuels were loaded in fine mesh gold baskets and suspended in the autoclaves. The autoclaves were filled with 800 ml of simplified granitic groundwater (10 mM NaCl, 2 mM $NaHCO_3$). The first autoclave was loaded with 10 g of iron powder (Alfa Aesar 10 µm mesh) at the bottom of the autoclave. In addition, two strips of iron foil (0.5 × 2 cm, 20 µm thickness) were suspended above the fuel basket. The second autoclave was loaded with 10 g of magnetite powder (Aldrich <5 µm mesh), of which 9 g were placed at the bottom of the autoclave. In addition, a small gold bucket with 1 gram of the magnetite powder was also suspended above the fuel basket. The autoclaves were equipped with a series of valves to enable gas sampling and syphoning of solution. Both autoclaves were sparged with Ar+0.003% CO_2 to eliminate residual air before being pressurized. The spent fuel iron corrosion autoclave was pressurized to 1 MPa and the magnetite powder autoclave to 2.3 MPa of Ar. Gas samples were analyzed by gas-MS (GAM 400). Sampling of the solution was typically performed in triplicate with the first sample used for flushing of the sampling line. The second two aliquots were centrifuged (RCF 74k g, 1 h) with the supernatant analyzed by ICP-MS (Perkin Elmer Elan DRC II and Nexion 350D). The analytical protocol was similar to that described in [27], although with adaptations. The analytical uncertainty depends on the isotope and concentration but generally falls in the range of ± 3–10%. The largest variation within duplicate or triplicate samples is typically associated with very low measured concentrations or redox sensitive elements. Selected samples were also analyzed for pH and total carbonate content. The dissolved Fe content was however not measured during the course of the experiments (would require additional sampled volume and analyti-

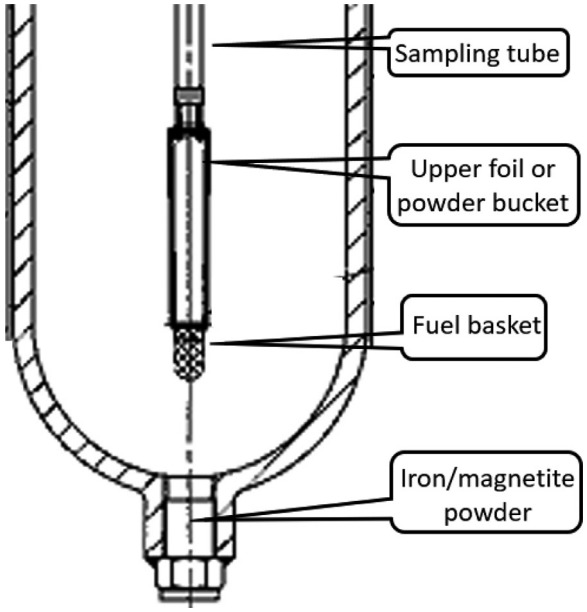

Fig. 1. Internal arrangement of the autoclaves.

cal work). Fig. 1 gives an overview of the internal arrangement in the autoclaves.

No refilling or exchange of either the gas phase or the solution was performed after samplings. The experiments were performed at room temperature (~20 °C). At the conclusion of the experiment, the autoclaves were opened inside a shielded glove box with inert atmosphere (<1 ppm O_2). The last solution sampling of the iron corrosion autoclave was performed at 1240 days duration, whereas the autoclave was opened inside the glovebox for extraction of solid samples after a total duration of 1250 days. In the case of the magnetite autoclave, the last sampling of solution was at 275 days duration after which the autoclave was opened. Samples of the extracted corrosion products were dried inside the glove box. Fractions were sealed under kapton foil and analyzed by powder XRD (Panalytical X'pert Pro). In the case of the iron corrosion autoclave, a sample was also sealed and analyzed by Raman spectrometry (Renishaw inVia Reflex). Samples of the iron corrosion products and corroded magnetite powder, including uncorroded blank samples, were also dried, weighed, dissolved in nitric acid and analyzed by ICP-MS to determine their radionuclide content. An inactive autoclave experiment was also performed under the same conditions as the experiment with iron powder, but with no spent nuclear fuel to assess the rate of hydrogen formation from iron corrosion in the absence of the spent fuel.

3. Results and discussion

3.1. Evolution of the gas phases in the autoclave experiments

Fig. 2 presents the evolution of hydrogen pressures in the autoclave with spent fuel and iron powder, as well as the results from the inactive autoclave without fuel. Nitrogen and oxygen concentrations were fluctuating near the quantification limit (low ppm range) throughout the iron corrosion experiment. Besides Ar and H_2, the mass spectra indicated no significant presence of other species than water vapor and CO_2 from the carbonate equilibrium (i.e. no methane formation from potentially interfering microbial contamination).

Hydrogen generation was observed in both cases containing iron powder, but when spent fuel was present, the production rate was higher. The rate was approximately linear and, for the autoclave with spent fuel, was about 8.5×10^{-5} mol H_2/day. Without spent fuel, the rate was about 2.2×10^{-5} mol H_2/day. The difference in production rate was sustained for over 1000 days. It is not evident that the difference was caused solely by water radiolysis, as the observed potential radiolysis component in hydrogen production rate is higher than what has previously been reported [9,28]. However, the conditions were different in those experiments. Another possible explanation for the higher hydrogen production rates seen here is a radiation-enhanced anaerobic iron corrosion effect, as observed in a steel corrosion study [20].

Table 1
Gas-MS results from the spent fuel autoclave with magnetite powder.

Time [d]	Pressure [kPa]	H_2 [ppm]	Ar [%]	O_2 [ppm]	N_2 [%]
5	1440	(28)	99.8	400	0.12
68	1240	(12)	99.8	162	0.12
224	1060	53	99.8	(8)	0.12

The third autoclave experiment in this study was also performed with the same type of spent fuel but with the iron powder substituted with magnetite powder. Table 1 gives the results of gas analysis from that experiment (the values in parenthesis are below the quantification limit). As can be seen, the gas phase is close to constant for the duration of the experiment, consisting of 99.8% Ar. The small and constant fraction of N_2 is attributed to residual air from the sparging of the system. The constant nitrogen level serves as a good indicator that the autoclave was leak tight. The oxygen content decreases to the quantification limit of the gas-MS method (the initial level of 400 ppm is mainly attributed to residual air at start-up). The hydrogen level was approximately constant near the quantification limit. No fission gas release or methane formation was detected in the gas phase.

Because neither oxygen nor hydrogen was found to increase in the autoclave with spent fuel and magnetite, it seems likely that the system was able to scavenge any gasses produced by radiolysis.

3.2. Characterization of the iron corrosion products

In the iron corrosion case, the hydrogen produced predominantly comes from anoxic corrosion of either ca 42% or ca 55% of the added iron, based either on the formation of Fe(II) or magnetite (Fe_3O_4). The observed changes in pH from 8.2 to 10.4 over the course of the 1240-day long experiment indicates that Fe(II) had formed. There was also a slow decrease in carbonate concentration, from 127 ppm to 62 ppm, which together with limited available carbonate excludes any significant precipitation of siderite ($FeCO_3$) or carbonate green rusts (mixed Fe(II),(III) layered double hydroxides). Anoxically dried and sealed iron corrosion products from the autoclave with spent fuel and corroding iron were analyzed with Raman spectroscopy. The resulting baseline-subtracted Raman spectra (Fig. 3, left) show that magnetite had formed in the experiment. The peak at 669 cm^{-1} is characteristic of magnetite [29]. Raman spectra collected from the inactive autoclave also indicate only magnetite formation (not shown). In addition, XRD measurements performed on the corroded iron from the active autoclave indicate magnetite and iron (Fig. 3, right), based on the relative intensity of magnetite [30] and iron references [31].

The results from the autoclave with spent fuel and iron powder, and the inactive autoclave with iron powder (and no spent fuel), are both consistent with evolution of hydrogen from anoxic corrosion of the metallic iron powder into magnetite. Because magnetite was found to be the major corrosion product, the third autoclave experiment was performed starting with spent fuel and magnetite powder instead of iron powder. The surface area of the added magnetite powder (10 g, 5 µm mesh) was estimated to be larger than the initial surface area in the iron corrosion case (10 g, 10 µm mesh

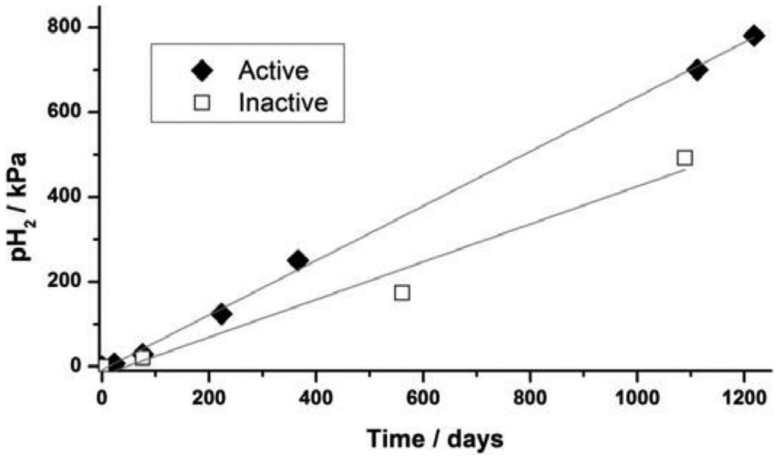

Fig. 2. Evolution of the hydrogen pressure in the autoclave with spent fuel and iron powder (filled diamonds), and the inactive reference autoclave with iron powder but without fuel (open squares). Figure from [11].

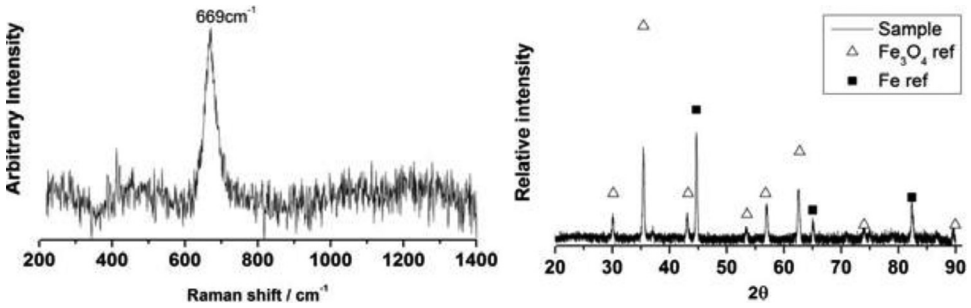

Fig. 3. Corrosion products in the autoclave with spent fuel and iron powder analyzed by Raman (left) and XRD (right). Figure from [11].

iron powder). Powder XRD with Rietveld refinement of the supplied magnetite powder confirmed it was 100% magnetite. Powder XRD sampling at the conclusion of the magnetite autoclave experiment after 275 days resulted in ~94% magnetite and 6% hematite, indicating partial oxidation of the magnetite powder during the experiment. The appearance of solutions and powders at the conclusion of the three experiments was very similar. The corroded powders were all dark gray to black, the powders quickly settled from the solution and were easily separated from the solution by magnetic decantation, yielding clear solutions. The pH and total carbonate levels did not change during the magnetite autoclave experiment, being steady at pH about 8.1 and 121 to 141 ppm carbonate.

3.3. Radionuclide concentrations in the aqueous phase of the iron corrosion autoclave

Fig. 4 shows the concentration evolution of selected redox sensitive radionuclides in the case of the autoclave with corroding iron powder and generation of hydrogen. The initial very fast rise in concentrations (peak concentrations in Fig. 4 at 2.6 days) can be attributed to release of pre-oxidized outer layers of the fuel matrix as noted in several other spent fuel studies [5–7,26,32]. The uranium concentration (U-238) then decreases to values of ~3×10^{-9} M or slightly lower within 76 days, in good agreement with the solubility limit of UO_2 (am) [33] expected under reducing conditions. Tc-99, Pu-239 and Np-237 also decrease to very low concentrations, which may be attributed to reductive precipitation. Pu-239 attains concentrations as low as ~1×10^{-11} M, with Np-237 decreasing to below 1×10^{-12} M (approaching the quantification limit). The concentrations thus appear to be lower than what could be obtained from reductive precipitation, being below the solubility of their tetravalent oxide forms, as observed also in other spent fuel leaching tests under hydrogen [5–7,26,32]. The reported solubility of NpO_2(s) is ~3×10^{-9} M [33,34], close to that of amorphous UO_2 [33], while Np concentrations in solution are about three orders of magnitude lower than those of uranium, in line with the roughly thousand times lower Np inventory in the spent fuel. This indicates that the reduced Np(IV) and Pu(IV) ions co-precipitate with U(IV) from solution to form a mixed oxide. This is expected, given the similarity of their ionic radii with eight coordination 0.96 Å Pu(IV), 0.98 Å Np(IV), 1.00 Å U(IV) [35] and of the fluorite type structures of their tetravalent oxides. The co-precipitation of NpO_2(s) with UO_2(s) has been reported in literature [36]. The composition of the mixed actinide oxide would reflect that of the pre-oxidized layer or of the spent fuel, i.e. it would contain over 100 times less Pu and about 1000 times less Np than U, which would agree with the measured concentrations in solution in case of an ideal solid solution. Am also follows a similar behavior to Np, as given by Am-243, although Am(III) would be expected as the predominant oxidation state. Molybdenum concentrations (Mo-100) also decrease by almost two orders of magnitude in the iron corrosion experiment. It should be pointed out that the 316L-alloy of the autoclave contains Mo. The Mo isotopic composition in solution (based on Mo-95, 96, 97, 98 and 100) was, however, found to be in agreement with the calculated spent fuel inventory, which has a very different isotopic composition from naturally occurring Mo, confirming that the major part of the Mo was released from the fuel. Mo is a potential redox-indicator. The predominant oxidized and soluble Mo form at the pH of 8 to 10 in the autoclave, the molybdate anion (MoO_4^{2-}), displays limited adsorption, requiring strongly reducing condition for its immobilization to occur [37]. It should however be pointed out that literature on Mo speciation and solubilities is scarce under reducing conditions [38].

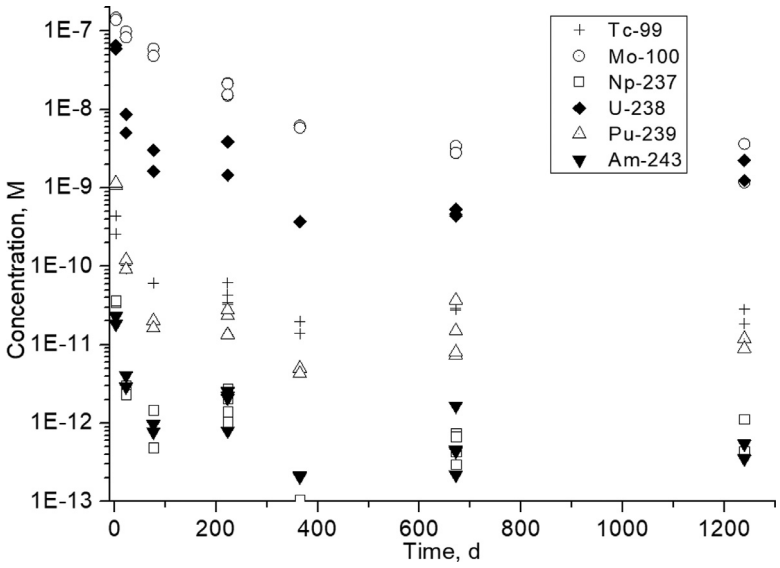

Fig. 4. Evolution of the redox sensitive species Tc-99, Mo-100, Np-237, U-238, Pu-239, and Am-243 in the autoclave with spent fuel and corroding iron.

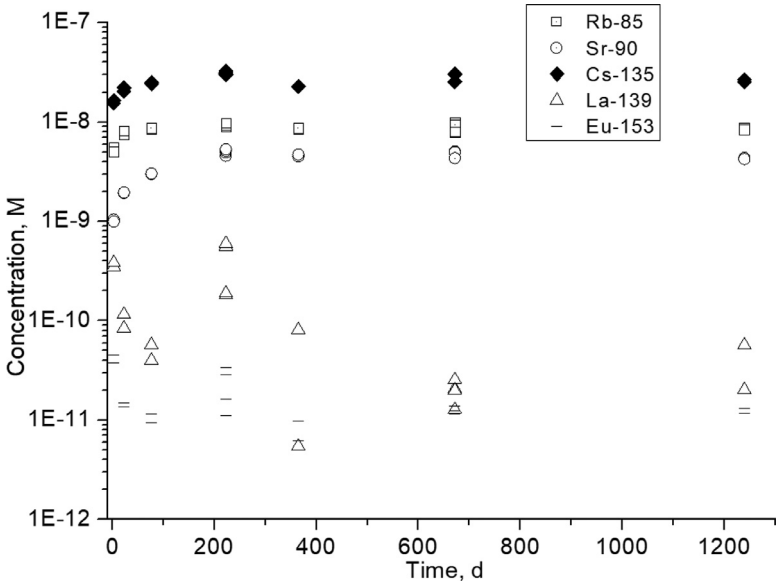

Fig. 5. Evolution of the non-redox sensitive species Rb-85, Sr-90, Cs-135, La-139, Eu-153 in the autoclave with spent fuel and corroding iron.

Although stable Mo concentrations were attained in other spent fuel leaching studies under hydrogen conditions [6,7], Mo did not decrease to the extent observed in the iron corrosion autoclave experiment. In [37] molybdate immobilization by Zero-Valent Iron (ZVI) as well as ZVI/magnetite/Fe(II) systems was studied, finding enhanced removal by the hybrid iron/magnetite system with cases of both Mo(VI) and Mo(V) species found on the surface (as evidenced by XPS). The observed Mo immobilization in the present case could thus potentially be attributed to the presence of the corroding iron surface rather than only from the generated hydrogen. In this case, immobilization should be read as a removal from solution either by reductive precipitation or by adsorption, given that the Mo speciation is unknown and that supporting literature on likely phases is scarce.

Fig. 5 shows the evolution of selected non-redox sensitive species in the iron corrosion autoclave. The rapid initial release of Cs, Rb and Sr is probably predominantly from pre-oxidized phases and the instant release fraction. From 223 days and onwards no further release appears to occur (a small decrease is even noted), indicating inhibition of matrix dissolution. Unlike Cs, Rb and Sr, which are expected to have very low affinity to adsorb on iron corrosion products, the decreasing concentrations of lanthanides La and Eu can probably be attributed to their stronger affinity to being adsorbed on the iron corrosion products [39]. Cs, Rb and Sr have very weak hydrolysis and adsorb to a much lesser extent than the lanthanides. Both hydrolysis and sorption refer to affinity for the OH-group, of water in the hydrolysis case, and of OH-groups on the mineral surface [40].

3.4. Radionuclide concentrations in the aqueous phase in the magnetite corrosion autoclave

Fig. 6 presents the evolution in concentrations of selected redox-sensitive species in the case of the spent fuel autoclave with magnetite powder. The U-238 concentration continuously increases, exceeding 2×10^{-5} M at 275 days, which is about four orders of magnitude higher than in the case of the autoclave with corroding iron and hydrogen generation (Fig. 4). This indicates con-

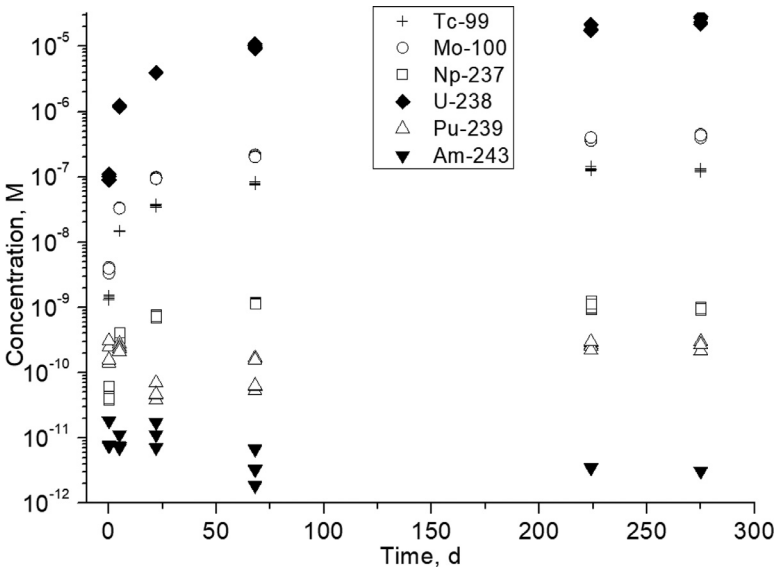

Fig. 6. Evolution of the redox sensitive species Tc-99, Mo-100, Np-237, U-238, Pu-239 and Am-243 in the autoclave with spent fuel and magnetite powder.

tinuous corrosion and dissolution of the uranium fuel matrix. The concentrations of Mo and Tc also increase with time with the Tc concentration being close to three orders of magnitude higher in the magnetite experiment at 275 days than in the iron corrosion autoclave. This indicates at least moderately oxidizing conditions in the magnetite case.

Interestingly, the concentration of Np-237 appears to stabilize at a level of ~1×10^{-9} M, with the Pu-239 concentration remaining below 3×10^{-10} M, potentially reflecting the larger tetravalent stability region of Pu under moderately oxidizing conditions. Am-243 also decreases to concentrations of $<1 \times 10^{-11}$ M. This behavior of Np and Pu has been observed also in other spent fuel leaching tests carried out in the presence of air or Ar atmospheres [41,42]. In spite of the apparently oxidizing conditions, the solid fuel is composed mainly by UO_2(s) containing uranium in its reduced form. Thermodynamically, U(IV) ions can reduce Np(V) and Pu(V), as shown by the large negative ΔG values of the corresponding inter-actinide redox reactions calculated from data in [33]:

$$U^{4+} + 2NpO_2^{+} + 4H^{+} \Rightarrow UO_2^{2+} + 2Np^{4+} + 2H_2O \quad \Delta G^{\circ} = -2163.1 \text{ kJ/mol}$$

$$U^{4+} + 2PuO_2^{+} + 4H^{+} \Rightarrow UO_2^{2+} + 2Pu^{4+} + 2H_2O \quad \Delta G^{\circ} = -1665.2 \text{ kJ/mol}$$

This also applies to UO_2(s). The reductive adsorption of Np(V) on UO_2(s) has been demonstrated experimentally [43]. This potential reduction on the UO_2(s) surface seems to be a plausible explanation for the relatively low concentrations of minor actinides in-spite of the rather high U concentration and moderately oxidizing conditions prevailing in the magnetite autoclave.

Fig. 7 shows the evolution of selected non-redox sensitive species in the magnetite autoclave. The releases of Cs-135, Sr-90 and Rb-85 in the magnetite autoclave are all higher than in the iron corrosion experiment. But concentrations are only less than an order of magnitude higher, which is noteworthy given the four orders of magnitude difference in uranium concentration between the two experiments (U being redox sensitive). The evolution of the concentration of lanthanides such as La-139 and Eu-153 in the magnetite experiment is similar to the iron corrosion case, which is expected given their strong tendency for adsorption to iron oxide surfaces.

3.5. Estimation of distribution coefficients, K_d of the iron oxides

In addition to the characterization of the corroded iron powder and the corroded magnetite, which resulted in magnetite being identified as the major corrosion product (and a small fraction of hematite identified in the corroded magnetite sample), samples of a few hundred mg of the corroded materials were also dried, weighed, dissolved and analyzed by ICP-MS for their radionuclide content per weight of material dissolved. For the iron corrosion autoclave, one of the two iron foils suspended above the spent fuel basket and portions of the corroded iron powder were retrieved from the autoclave and dissolved. The corroded iron powder in the bottom of the autoclave had settled in the narrower bottom neck of the autoclave (Fig. 1). One of the portions was retrieved from the approximate upper layer, while the other portion was taken with more of the material retrieved from deeper layers farther from the interface to the solution. The radionuclide content in fractions of mass of the samples was multiplied by the estimated corroded amount of material in the autoclaves. As the amount of hydrogen evolved suggested about 40% of the added iron had corroded in the course of the experiment, the mass of corroded iron powder was assumed to be 4 g (out of 10 g added). This assumption was made both for the cases of the sample from the top layer and for the bottom layer. For the iron foil, the mass of the foil was used. The concentration of radionuclides at the termination of the experiment was used to calculate approximate distributions coefficients, K_d-values (ml/g). In the case of the magnetite autoclave, a sample was taken and dissolved from the open bucket suspended at few centimeters above the basket with spent fuel. The autoclave also contained magnetite powder in the bottom of the autoclave a few centimeters below the fuel basket. Table 2 presents the approximate K_d-values for the samples in the experiments. A species with a low K_d-value displays limited adsorption and high aqueous mobility, whereas a high value is consistent with reductive precipitation or strong adsorption and limited mobility.

The K_d values of Cs for the corroded iron foil and the top layer of the corroded iron powder agree with the K_d-value of 9 ml/g (at pH 9) for magnetite reported by Torstenfelt et al. [44]. The bottom layer of the corroded iron powder, however, results in low K_d-values, indicating a concentration gradient through the iron powder. A similar situation appears to be present in the magnetite powder autoclave, resulting in low Cs K_d-values if all the 10 g of

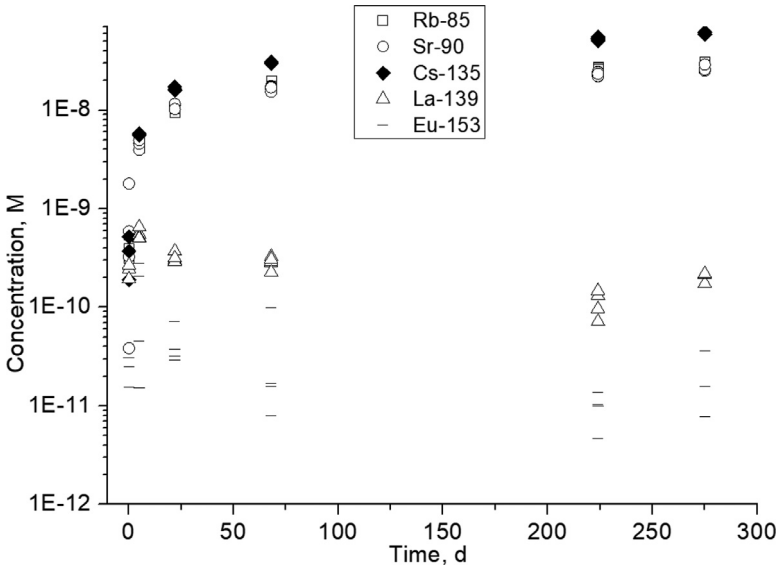

Fig. 7. Evolution of the non-redox sensitive species Rb-85, Sr-90, Cs-135, La-139 and Eu-153 in the autoclave with spent fuel and magnetite.

Table 2
Approximate K_d-values for the samples in the experiments.

K_d ml/g	Corroded iron foil	Top layer corroded iron powder	Bottom layer corroded iron powder	Corroded magnetite powder 10 g basis	Corroded magnetite powder 2 g basis
Rb-85	1.4×10^1	1.4×10^1	1.0×10^0	2.0×10^0	1.1×10^1
Rb-87	1.4×10^1	1.4×10^1	1.0×10^0	2.0×10^0	1.1×10^1
Sr-88	2.3×10^1	8.1×10^1	1.5×10^1	8.0×10^0	3.9×10^1
Sr-90	3.7×10^2	–	–	1.4×10^1	6.9×10^1
Mo-100	1.6×10^3	2.5×10^3	1.9×10^3	–	–
Tc-99	1.9×10^4	8.6×10^4	1.0×10^4	2.0×10^{-1}	1.0×10^0
Cs-133	1.3×10^1	8.0×10^0	1.0×10^0	2.0×10^0	1.0×10^1
Cs-135	6.0×10^0	9.0×10^0	1.0×10^0	2.0×10^0	9.0×10^0
Cs-137	9.0×10^0	1.0×10^1	4.0×10^0	1.0×10^0	4.0×10^0
La-139	1.9×10^4	4.9×10^4	4.0×10^3	9.4×10^3	4.7×10^4
Pr-141	6.6×10^4	1.8×10^5	1.5×10^4	9.2×10^3	4.6×10^4
Nd-144	6.2×10^4	1.8×10^5	1.3×10^4	1.9×10^4	9.6×10^4
Eu-153	5.2×10^3	1.3×10^4	7.9×10^2	8.3×10^2	4.2×10^3
Gd-156	4.0×10^4	1.4×10^5	1.1×10^4	1.1×10^3	5.5×10^3
U-238	8.5×10^4	1.9×10^5	1.9×10^4	1.0×10^0	5.0×10^0
Np-237	1.6×10^5	3.1×10^5	2.8×10^4	1.2×10^1	6.1×10^1
Pu-239	1.1×10^5	3.3×10^5	2.8×10^4	1.2×10^1	5.9×10^1
Am-243	5.5×10^4	1.8×10^5	1.5×10^4	4.6×10^2	2.3×10^3

magnetite added is used in the calculation. However, if one assumes that only about 20% of the added powder is in equilibrium with the aqueous solution, then a Cs K_d-value of about 9 ml/g is also obtained, which is consistent for both hematite and magnetite [44]. In the case of Sr, the results based on Sr-88 are probably more accurate, as evaluating Sr-90 proved difficult in the case of the dissolved iron oxides (highly variable content of interfering trace elements such as Zr-90). The Sr-88 K_d-values in Table 2 fall in the range from 8 to 81 ml/g, which could be attributed to pH effects given the carbonate-containing solution. At the end of the iron corrosion experiment, the pH was 10.4 and at such conditions Sr could be expected to precipitate as $SrCO_3$, resulting in higher K_d-values [44], whereas the end pH was ~8.1 in the magnetite autoclave, which should result in lower values. The obtained results for the iron corrosion autoclave agree with the range of K_d-values presented in the review paper by Li and Kaplan for sorption coefficients of Pu, U, Np, Am and Tc on Fe hydroxides and oxides [45]. The very low K_d-values of Tc for the magnetite autoclave are also in line with the TcO_4^- sorption results in [45]. The many orders of magnitude lower U, Np and Pu K_d-values of the magnetite autoclave compared with the iron corrosion autoclave are also in line with the expected low K_d-values of actinides in their higher oxidation states stabilized by formation of anionic carbonate complexes [45]. The K_d value of Am (being trivalent) is, however, closer to that of the lanthanides, and is about two orders of magnitude higher than those of the other actinides in the magnetite case. Given the experimental difficulties with the potential for strong concentration gradients inside the sampled materials and the unknown degree of sorption or reductive precipitation on the stainless-steel walls of the autoclave, the obtained values should be treated cautiously. One can, however, make some observations. In the case of weakly adsorbing redox-insensitive elements such as Rb and Cs, the obtained K_d-values are largely similar for both the iron corrosion autoclave and the magnetite autoclave. This also applies to the strongly adsorbing lanthanides. Some important differences can be seen for Mo and Tc. In the iron corrosion autoclave, the high Mo and Tc K_d-values are consistent with immobilization of Mo-oxides and TcO_2. The solids in the magnetite autoclave, however, resulted in no or trace amounts of Mo and Tc, indicating no reduction on the iron oxides and very weak adsorption, consistent with molybdate and pertechnetate presence, indicative of oxidizing conditions. The actinides also display a similar behav-

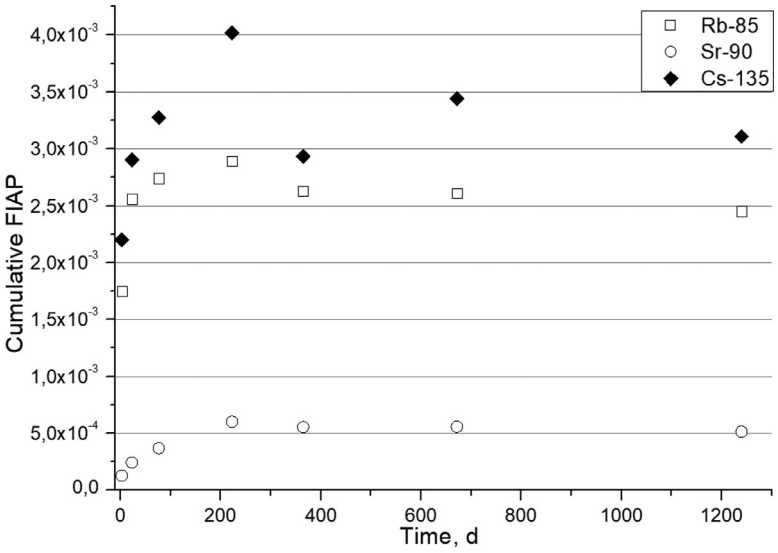

Fig. 8. Cumulative fraction of inventory in the aqueous phase for Rb-85, Sr-90 and Cs-135 in the iron corrosion autoclave.

ior (trivalent Am being the exception) of weak adsorption in the magnetite autoclave. The U K_d-value obtained is in fair agreement with the U K_d value of 4 ml/g for magnetite reported in [46]. The several orders of magnitude higher actinide K_d-values in the iron corrosion autoclave are consistent with reductive precipitation on the iron surfaces. Because the top layer of the corroded iron powder displays the highest actinide K_d-values, and because it was situated directly below the suspended spent fuel basket, one could suspect that fuel grains might have fallen onto the corroding powder causing an overestimated actinide content. However, given the Rb and Cs K_d-values of the top corroded layer and the corroded iron foil (which was suspended above the fuel) being close to each other, and the good match to literature K_d-values, the results do not support accidental inclusion of intact grains of fuel in the corroded iron samples. If grains of fuel not being in equilibrium with the autoclave solution had been sampled accidentally, the Cs and Rb would also have displayed uncharacteristically high K_d-values (as most of the Cs and Rb inventory is still contained inside the fuel).

3.6. Fractions of inventory in the aqueous phase and fractional release rates

Fig. 8 presents the cumulative Fraction of Inventory in the Aqueous Phase (FIAP) for Rb-85, Sr-90 and Cs-135 in the iron corrosion autoclave. The fraction removed due to each sample aliquot was considered (no replenishment of autoclave solution between samplings) and the cumulative FIAP was calculated from the average concentration of the aliquots of each sampling occasion and their volumes.

In Fig. 8, the Sr-90 FIAP reaches a maximum of 6×10^{-4} at 223 days. Rb-85 and Cs-135 follow the same trend with a maximum of 2.9×10^{-3} for Rb-85 and 4×10^{-3} for Cs-135 at 223 days. Past 223 days all three radionuclides display constant or even slightly decreasing cumulative FIAP, consistent with the slightly decreasing concentrations in Fig. 5 (note linear vs logarithmic y-axis). This behavior is further illustrated in Fig. 9, which gives the fractional release rates per day of Rb-85, Sr-90 and Cs-135. Past 223 days the release rates fluctuate around zero. A zero rate would be consistent with exhaustion of the instant release fraction and complete inhibition of matrix dissolution. Such a result is, however, practically unobtainable as even the slightest analytical error would cause a result that fluctuates near zero, as was observed. It should also be pointed out that the slightly decreasing cumulative FIAP trend observed in Fig. 8 might be attributed to continuous adsorption of radionuclides on the corroding iron surfaces, as its surface area likely increases with time due to the sustained hydrogen generating corrosion process.

Fig. 10 presents the cumulative fraction of inventory in the aqueous phase for Rb-85, Sr-90 and Cs-135 in the magnetite autoclave. Although the duration of this experiment was shorter, the FIAP continuously increases out to the end point at 275 days, reaching cumulative FIAP results of 3.1×10^{-3} for Sr-90, 7.7×10^{-3} for Rb-85 and 6.6×10^{-3} for Cs-135. Fig. 11 gives the corresponding fractional release rates per day calculated from the cumulative FIAP for the magnetite autoclave. For the last two sampling occasions at 224 and 275 days the rates fall in the range of 4×10^{-6} to 2×10^{-5} per day, which are almost an order of magnitude faster than the corresponding case for the iron corrosion autoclave at 223 days' duration. Together with the increasing uranium concentration (Fig. 6), this indicates that the fuel matrix continued to corrode and dissolve throughout the magnetite autoclave experiment.

3.7. Approximate fractions of inventory in the solid corrosion products

Table 3 presents cumulative Fractions of Inventory in the Aqueous Phase (FIAP) for the iron corrosion experiment with hydrogen evolution (1240 days), and for the shorter duration magnetite corrosion experiment (275 days duration). Care must be given in the interpretation of the results because FIAP values are prone to underestimate the total release of redox sensitive or strongly adsorbing species, in which case large fractions of the radionuclides released from the fuel may have been reductively precipitated or adsorbed on the iron oxide powders, inner surfaces of the autoclaves or even on the fuel surface itself. It should also be noted that Table 3 does not include radionuclides released during prewashing of the fuels prior to its introduction in the autoclave. A general observation from Table 3 is that the FIAP for all radionuclides is higher in the magnetite powder experiment despite its much shorter duration of 275 days versus the 1240 days of the iron corrosion experiment. This is especially the case for the redox sensitive radionuclides (Mo, Tc, U, Np, Pu), by several orders of magnitude. Because samples of the corroded iron indicated strong radionuclide concentration gradients in the corroded materials, estimating total radionuclide releases (FIAP + inventory adsorbed or

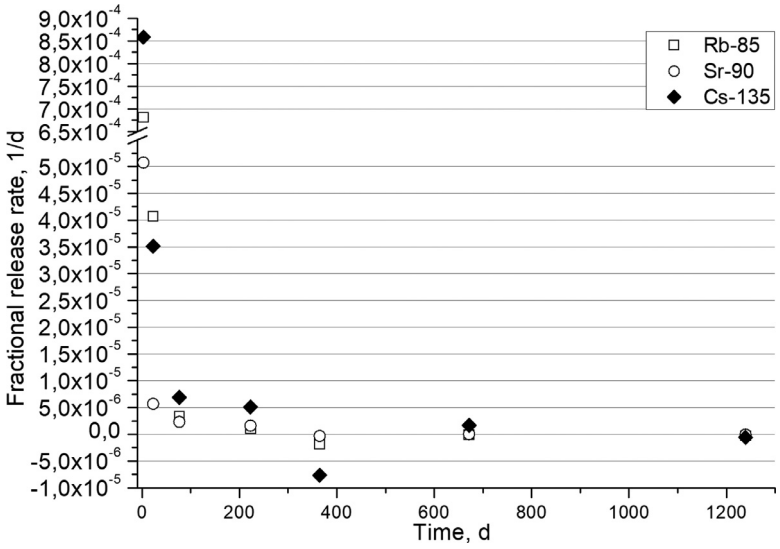

Fig. 9. Fractional release rates, 1/d for Rb-85, Sr-90 and Cs-135 in the iron corrosion autoclave.

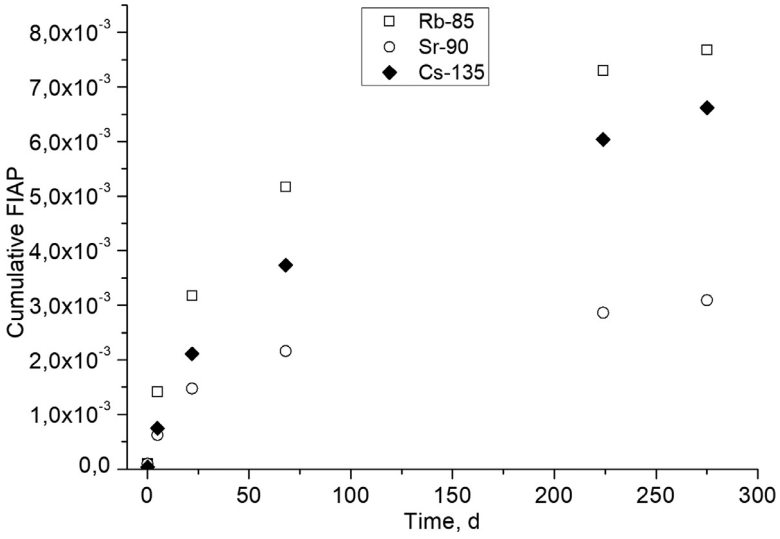

Fig. 10. Cumulative fraction of inventory in the aqueous phase for Rb-85, Sr-90 and Cs-135 in the magnetite autoclave.

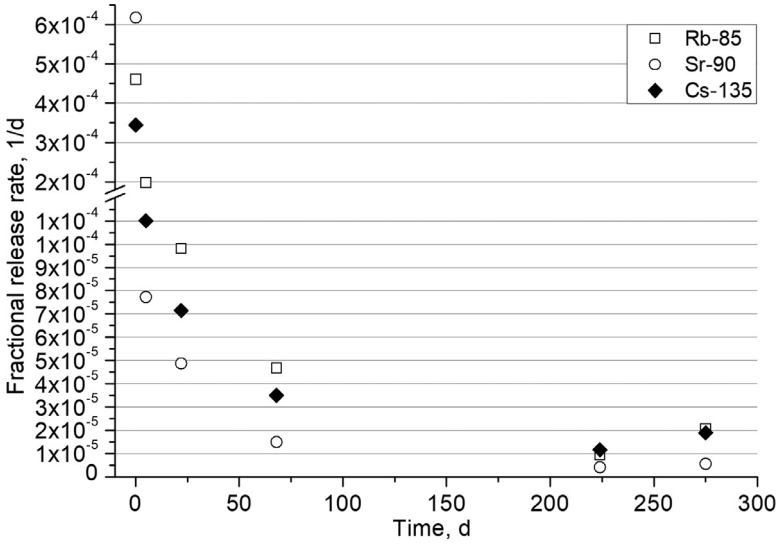

Fig. 11. Fractional release rates, 1/d for Rb-85, Sr-90 and Cs-135 in the magnetite autoclave.

Table 3
In autoclave cumulative FIAP and estimated inventory in the iron oxides.

	FIAP iron corrosion experiment (1240 d)	Inventory fraction Iron corrosion, top layer 4 gram basis	Inventory fraction iron corrosion, bottom layer 4 gram basis	FIAP magnetite corrosion experiment (275 d)	Inventory fraction magnetite powder, 10 gram basis	Inventory fraction magnetite powder, 2 gram basis
Rb-85	2.5×10^{-3}	8.0×10^{-4}	5.9×10^{-5}	7.7×10^{-3}	2.6×10^{-3}	5.1×10^{-4}
Rb-87	1.9×10^{-3}	6.3×10^{-4}	4.6×10^{-5}	6.0×10^{-3}	2.0×10^{-3}	4.1×-10^{-4}
Sr-88	5.3×10^{-4}	9.9×10^{-4}	1.9×10^{-4}	2.9×10^{-3}	3.5×10^{-3}	7.1×10^{-4}
Sr-90	5.2×10^{-4}	0	0	3.1×10^{-3}	6.8×10^{-3}	1.4×10^{-3}
Mo-100	8.4×10^{-5}	4.8×10^{-3}	3.6×10^{-3}	1.3×10^{-2}	0	0
Tc-99	9.8×10^{-7}	1.9×10^{-3}	2.3×10^{-4}	4.9×10^{-3}	1.7×10^{-4}	3.5×10^{-5}
Cs-133	3.2×10^{-3}	5.9×10^{-4}	7.5×10^{-5}	6.7×10^{-3}	2.0×10^{-3}	4.0×10^{-4}
Cs-135	3.1×10^{-3}	6.6×10^{-4}	1.1×10^{-4}	6.6×10^{-3}	1.9×10^{-3}	3.8×10^{-4}
Cs-137	3.2×10^{-3}	7.5×10^{-4}	2.8×10^{-4}	6.0×10^{-3}	8.2×10^{-4}	1.6×10^{-4}
La-139	1.4×10^{-6}	1.6×10^{-3}	1.3×10^{-4}	7.0×10^{-6}	1.0×10^{-2}	2.1×10^{-3}
Pr-141	$3.9 \times 10–^{7}$	1.6×10^{-3}	1.3×10^{-4}	2.5×10^{-6}	3.7×10^{-3}	7.4×10^{-4}
Nd-144	4.4×10^{-7}	1.8×10^{-3}	1.3×10^{-4}	4.3×10^{-6}	1.3×10^{-2}	2.6×10^{-3}
Eu-153	$5.2 \times 10–^{6}$	1.6×10^{-3}	9.5×10^{-5}	5.7×10^{-6}	7.6×10^{-4}	1.5×10^{-4}
Gd-156	$6.0 \times 10–^{7}$	1.9×10^{-3}	1.4×10^{-4}	2.7×10^{-5}	4.9×10^{-3}	9.8×10^{-4}
U-238	1.8×10^{-7}	8.1×10^{-4}	8.2×10^{-5}	2.4×10^{-3}	3.7×10^{-4}	7.3×10^{-5}
Np-237	1.4×10^{-7}	1.0×10^{-3}	9.1×10^{-5}	1.7×10^{-4}	3.2×10^{-4}	6.3×10^{-5}
Pu-239	2.0×10^{-7}	1.5×10^{-3}	1.2×10^{-4}	4.7×10^{-6}	8.6×10^{-6}	1.7×10^{-6}
Am-243	2.5×10^{-7}	1.0×10^{-3}	7.6×10^{-5}	4.2×10^{-7}	2.8×10^{-5}	5.5×10^{-6}

reductively precipitated) is precarious, even more so as the inner surfaces of the autoclaves were not investigated. Nevertheless, it appears the inventory of sparingly adsorbing non-redox sensitive radionuclides Rb, Sr and Cs is higher in the magnetite powders compared with the corroded iron powder. This also largely applies to the strongly adsorbing lanthanides. Major differences are seen for Mo with all molybdenum found in solution (Mo FIAP ~1.3×10^{-2}) for the magnetite case. Meanwhile, very little Mo was found in solution, but an inventory fraction of ~4–5 $\times$ 10^{-3} was seen in the iron corrosion case, in both the top and bottom corrosion layers. This may indicate that Mo was more homogeneously distributed in the corroded iron powders, potentially due to the stability of the highly mobile molybdate anion, enabling it to diffuse far into the corroding iron powders before being immobilized. No Mo could be detected in the solids from the magnetite autoclave. The case for Tc is similar, although more Tc was found in the outer layers of the corroded iron powders, with a small fraction of Tc also found in the magnetite powder, in line with the expected redox behavior of pertechnetate compared with molybdate. Approximate total U releases (FIAP + inventory in corroded solids) was higher in the magnetite autoclave, with most of the U found in solution in the magnetite powder case and most of the U found in the solids in the iron powder autoclave, as would be expected for reducing versus at least mildly oxidizing conditions.

However, if one estimates the combined FIAP and the inventory fractions found in the powders for Np, Pu and Am, the combined releases appear to be higher in the autoclave with corroded iron powder than in the magnetite case. One must, however, stress that such conclusions are precarious, as the inner surfaces of the autoclave vessel itself were not investigated (although the two autoclaves are of the same make and dimensions). Higher Pu and Np releases in the iron corrosion case could possibly be explained by the continuously corroding iron powder with hydrogen generation in the iron corrosion autoclave. This causes strongly reducing conditions forcing Np and Pu to their sparingly soluble tetravalent state (Am has a large trivalent stability range and is not expected to be redox-sensitive under these conditions). The longer duration and constantly increasing surface of new iron corrosion products could thus continue to adsorb species such as tetravalent actinides, leading to a small flux from the fuel surface to the corroding iron surfaces. This could lead to concentrations below the solubility of the diffusing species, if the rate of adsorption at the corroding iron surface was higher than the dissolution rate at the fuel surface. In the magnetite autoclave (likely more oxidizing conditions), the surface does not appear to evolve in the same way, with only limited oxidation of the magnetite to hematite being observed. This likely does not increase or change the surface appreciably with hematite having similar K_d-values to magnetite [45]. The high aqueous U and Tc concentrations in the magnetite case are also consistent with oxidized negatively charged uranyl carbonate complexes and pertechnetate, which do not readily adsorb onto iron oxides. The higher concentrations of U and Tc also probably exclude significant concentrations of dissolved Fe(II), a strong reductant. Given the observed formation of the Fe(III) oxide hematite in the magnetite powder, this offers further evidence that the redox conditions in the magnetite autoclave evolved in such a way that Fe(II) could probably only act as a reductant at the magnetite surface, with limited impact on the conditions in the bulk of the solution, or at the fuel surface. It should also be noted that the gold baskets containing the fuel were found to be pristine at the conclusion of the autoclave experiments, with no visual evidence of precipitates such as Fe(III)-oxides.

4. Summary and conclusions

The presented work includes results from three autoclave experiments. Anoxic iron corrosion experiments with and without spent nuclear fuel caused sustained hydrogen generation and formation of magnetite as the dominant corrosion product. In order to attempt to isolate the role of the evolved hydrogen from that of the iron corrosion product, magnetite, a spent fuel experiment was also performed under the same initial conditions except with magnetite powder as the starting material. The magnetite experiment led to sustained release of radionuclides and orders of magnitude higher concentrations of redox-sensitive radionuclides, Mo, Tc and U, compared with the iron corrosion case. However, the experiment with spent nuclear fuel in the presence of corroding iron and simultaneous hydrogen generation by corrosion points to inhibition of fuel matrix corrosion ~223 days into the experiment. The main evidence is the termination of Cs, Sr and Rb release and the decrease of the uranium concentration to UO_2 (am) solubility-controlled level in the iron corrosion case. Concentrations of Np and Pu also decreased to exceedingly low levels in the range of 1×10^{-12} to 1×10^{-11} M in the case of the iron corrosion autoclave. Np and Pu still held at levels of 1×10^{-9} to 1×10^{-10} in the magnetite case, indicating Np and Pu solubility control by

their tetravalent phases in both autoclaves despite the high concentrations of U in the magnetite autoclave. A second observation is that no passivation of the hydrogen generating iron corrosion appears to occur over its three years of duration. The hydrogen partial pressure at 223 days was approximately 120 kPa H_2, which corresponds to ~1 mM of dissolved hydrogen in the aqueous phase. This hydrogen level is very close to the hydrogen concentration at which spent fuel corrosion and dissolution inhibition was also observed in the study by Ekeroth et al. [7] under very similar experimental conditions but in the absence of iron. Under these conditions, it thus appears that a hydrogen partial pressure of ~100 kPa suppresses further fuel matrix oxidation and dissolution. In the current experiment, the hydrogen was generated by the corrosion of iron powder. Although it appears the generation of hydrogen is the main factor in the observed inhibition of spent fuel corrosion, it should be noted that the anoxically corroding iron and the generation of Fe(II) also appear to present additional immobilization pathways, as was observed by the decreasing Mo concentrations that were not observed in previous experiments under hydrogen conditions.

Data availability

The raw/processed data required to reproduce these findings cannot be shared at this time due to technical or time limitations.

Declaration of Competing Interest

The authors declare that they have no known competing financial interests or personal relationships that could have appeared to influence the work reported in this paper.

CRediT authorship contribution statement

A. Puranen: Writing - original draft, Writing - review & editing. **A. Barreiro:** Investigation, Validation, Writing - review & editing. **L.-Z. Evins:** Conceptualization, Writing - review & editing, Project administration, Funding acquisition. **K. Spahiu:** Supervision, Writing - original draft, Writing - review & editing.

Acknowledgment

The authors would like to thank C. Askeljung, M. Granfors and V. Flygare for help with hot cell laboratory work as well as R. Gejland for help with radiation protection work at Studsvik Nuclear AB. The Swedish Nuclear Fuel and Waste Management Company, SKB, is acknowledged for financial support.

References

[1] Fuel and Canister Process Report for the Safety Assessment SR-Can. SKB Technical Report, TR-06-22 (2006)
[2] Criticality Effects of Long-Term Changes in Material Compositions and Geometry in Disposal Canisters. SKB Technical Report, TR-16-06 (2016)
[3] B. Bonin, M. Colin, A. Dutfoy, Pressure building during the early stages of gas production in a radioactive waste repository, J. Nucl. Mater. 281 (2000) 1–14, doi:10.1016/S0022-3115(00)00184-7.
[4] Jonsson M., Radiation Effects on Materials Used in Geological Repositories for Spent Nuclear Fuel, ISRN Materials Science, 2012, Article ID 639520, 13 pages, 2012.
[5] P. Fors, P. Carbol, S. Van Winckel, K. Spahiu, Corrosion of high burn-up structured UO_2 fuel in presence of dissolved H_2, J. Nucl. Mater. 394 (2009) 1–8, doi:10.1016/j.jnucmat.2009.07.004.
[6] A. Puranen, O. Roth, L-Z. Evins, K. Spahiu, Aqueous leaching of high burnup UO_2 fuel under hydrogen conditions, in: MRS Advances Scientific Basis for Nuclear Waste Management XLI, 3, Materials Research Society, 2018, pp. 1013–1018, doi:10.1557/adv.2018.273.
[7] E. Ekeroth, M. Granfors, D. Schild, K. Spahiu, The effect of temperature and fuel surface area on spent nuclear fuel dissolution kinetics under H_2 atmosphere, J. Nucl. Mater. 531 (2020) 151981, doi:10.1016/j.jnucmat.2019.151981.
[8] D. Cui, E. Ekeroth, P. Fors, K. Spahiu, Surface Mediated Processes in the Interaction of Spent Fuel or alpha-doped UO_2 with H_2, MRS Symp. Proc. 1104 (2008) 87–99, doi:10.1557/PROC-1104-NN03-05.
[9] A. Loida, M. Kelm, B. Kienzler, H. Geckeis, A. Bauer, The Effect of Nearfield Constraints on the Corrosion Behavior of High Burnup Spent Fuel, Mat. Res. Soc. Symp. Proc. 932 (72.1) (2006), doi:10.1557/PROC-932-72.1.
[10] A. Loida, V. Metz, B. Kienzler, H. Geckeis, Radionuclide release from high burnup spent fuel during corrosion in salt brine in the presence of hydrogen overpressure, J. Nucl. Mater. 346 (2005) 24–31, doi:10.1016/j.jnucmat.2005.05.020.
[11] A. Puranen, A. Barreiro, L-Z. Evins, K. Spahiu, Spent Fuel Leaching in the Presence of Corroding Iron, in: MRS Advances Scientific Basis for Nuclear Waste Management XL, 2, Materials Research Society, 2017, pp. 681–686, doi:10.1557/adv.2016.679.
[12] B. Grambow, A. Loida, P. Dressier, H. Geckeis, J. Gago, I. Casas, J. de Pablo, J. Gimenez, M.E. Torrero, Long-term safety of radioactive waste disposal: chemical reaction of fabricated and high burnup spent fuel with saline brines, Forschungszentrum Karlsruhe, Wissenschaftliche Berichte, 1996 FZKA 5702.
[13] P. Carbol, J. Cobos-Sabate, C. Ronchi, V. Rondinella, D.H. Wegen, T. Wiss, The Effect of Dissolved Hydrogen on the Dissolution of 233U Doped UO_2(s), High Burnup Spent Fuel and MOX Fuel, SKB Technical Report TR 05-09, (2005).
[14] M. Odorowski, C. Jegou, L De Windt, V. Broudic, G. Jouan, S. Peuget, C. Martin, Effect of metallic iron on the oxidative dissolution of UO_2 doped with a radioactive alpha emitter in synthetic Callovian-Oxfordian groundwater, Geochim. Cosmochim. Acta 219 (2017) 1–21, doi:10.1016/j.gca.2017.08.043.
[15] M. Saheb, D. Neff, Ph. Dillmann, H. Matthiesen, E. Foy, Long-term corrosion behaviour of low-carbon steel in anoxic environment: Characterisation of archaeological artefacts, J. Nucl. Mater. 379 (2008) 118–123, doi:10.1016/j.jnucmat.2008.06.019.
[16] T. Ishikawa, Y. Kondo, A. Yasukawa, K. Kandori, Formation of magnetite in the presence of ferric oxyhydroxides, Corros. Sci. 40 (1998) 1239–1251, doi:10.1016/S0010-938X(98)00045-6.
[17] C. Ruby, A. Aissa, A. Géhin, J. Cortot, M. Abdelmoula, J.-M.R. Génin, Green rusts synthesis by coprecipitation of Fe^{II}–Fe^{III} ions and mass-balance diagram, C.R. Geosci. 338 (2006) 420–432, doi:10.1016/j.crte.2006.04.008.
[18] K. Ritter, M.S. Odziemkowski, R.W. Gillham, An in situ study of the role of surface films on granular iron in the permeable iron wall technology, J. Contam. Hydrol. 55 (2002) 87–111, doi:10.1016/S0169-7722(01)00187-5.
[19] N.R. Smart, D.J. Blackwood, L. Werme, The anaerobic corrosion of carbon steel and cast iron in artificial groundwaters, SKB Technical Report TR-01-22 (2001).
[20] N.R Smart, A.P. Rance, L.O Werme, The effect of radiation on the anaerobic corrosion of steel, J. Nucl. Mater. 379 (2008) 97–104, doi:10.1016/j.jnucmat.2008.06.007.
[21] R. Ewing, Long-term storage of spent nuclear fuel, Nature Mater. 14 (2015) 252–257, doi:10.1038/nmat4226.
[22] L. Wu, Z. Qin, D.S. Shoesmith, An improved model for the corrosion of used nuclear fuel inside a failed waste container under permanent disposal conditions, Corros. Sci. 84 (2014) 85–95, doi:10.1016/j.corsci.2014.03.019.
[23] L. Bauhn, N. Hansson, C. Ekberg, P. Fors, K. Spahiu, The fate of hydroxyl radicals produced during H_2O_2 decomposition on a SIMFUEL surface in the presence of dissolved hydrogen, J. Nucl. Mater. 507 (2018) 38–43, doi:10.1016/j.jnucmat.2018.04.028.
[24] D.W. Shoesmith, Fuel corrosion processes under waste disposal conditions, J. Nucl. Mater. 282 (2000) 1–31, doi:10.1016/S0022-3115(00)00392-5.
[25] M. Trummer, O. Roth, M. Jansson, H_2 inhibition of radiation induced dissolution of spent nuclear fuel, J. Nucl. Mater. 383 (2009) 226–230, doi:10.1016/j.jnucmat.2008.09.021.
[26] K. Spahiu, D. Cui, M. Lundström, The fate of radiolytic oxidants during spent fuel leaching in the presence of dissolved near field hydrogen, Radiochim. Acta 92 (2004) 625–629, doi:10.1524/ract.92.9.625.54990.
[27] S. Röllin, K. Spahiu, U.B. Eklund, Determination of dissolution rates of spent fuel in carbonate solutions under different redox conditions with a flow-through experiment, J. Nucl. Mater. 297 (2001) 231–243, doi:10.1016/S0022-3115(01)00645-6.
[28] J. Bruno, E. Cera, M. Grivé, L. Duro, T. Eriksen, Experimental determination and chemical modelling of radiolytic processes at the spent fuel/water interface. Experiments carried out in carbonate solutions in absence and presence of chloride, SKB Technical Report TR-03-03 (2003).
[29] D.L.A. De Faria, S Venancio Silva, M.T. De Oliviera, Raman microspectroscopy of some iron oxides and oxyhydroxides, J. Raman Spectrosc. 28 (1997) 873–878.
[30] G.A. Harcourt, Tables for the identification of ore minerals by x-ray powder patterns, Am. Mineral 27 (1942) 90.
[31] H.E. Swanson, Standard X-ray Diffraction Powder Patterns, Natl. Bur. Stand. (U.S.), Circ. 539 (1955) IV3.
[32] P. Carbol, P. Fors, S. Van Winckel, K. Spahiu, Corrosion of irradiated MOX fuel in presence of dissolved H_2, J. Nucl. Mater. 392 (2009) 45–54, doi:10.1016/j.jnucmat.2009.03.044.
[33] R. Guillamont, et al., Update on the Chemical Thermodynamics of U, Np, Pu, Am and Tc, OECD NEA, Elsevier, 2003.
[34] T. Eriksen, P. Ndalamba, D. Cui, J. Bruno, M. Caceci, K. Spahiu, Solubility of the redox-sensitive radionuclides 99Tc and 237Np under reducing conditions in neutral to alkaline solutions. Effect of carbonate, SKB Technical Report TR 93-18, (1993).
[35] D. Rai, N. Hess, M. Yui, A. Felmy, D. Moore, Thermodynamics and solubility of $(U_xNp_{1-x})O_2$(am) solid solution in the carbonate system, Radiochim. Acta 92 (2004) 527–535, doi:10.1524/ract.92.9.527.54995.
[36] R.D. Shannon, Revised effective ionic radii and systematic studies of in-

teratomic distances in halides and chalcogenides, Acta Cryst. A 32 (1976) 751–767.
[37] Y.H. Huang, C. Tang, H. Zeng, Removing molybdate from water using a hybridized zero-valent iron/magnetite/Fe(II) treatment system, Chem. Eng. J. 200 (2012) 257–263, doi:10.1016/j.cej.2012.06.047.
[38] P.L. Smedely, D.G. Kinniburgh, Molybdenum in natural waters: A review of occurrence, distributions and controls, Appl. Geochem. 84 (2017) 387–432, doi:10.1016/j.apgeochem.2017.05.008.
[39] D.A. Dzombak, F.M.M. Morel, Surface Complexation Modeling: Hydrous Ferric Oxide, John Wiley & Sons, 1990.
[40] C.F. Baes, R.E. Mesmer, The Hydrolysis of Cations, Wiley, 1976.
[41] L.O. Werme, K. Spahiu, Direct disposal of spent nuclear fuel: comparison between experimental and modelled actinide solubiluties in natural waters, J. Alloys Compd. 271-273 (1998) 194–200, doi:10.1016/S0925-8388(98)00053-X.
[42] H.-U. Zwicky, J. Low, E. Ekeroth, Corrosion studies with high burnup light water reactor fuel. Release of nuclides into simulated groundwater during accumulated contact time of up to two years, SKB Technical Report TR-11-03 (2011).
[43] Y. Albinsson, H. Nilsson, A-M. Jakobsson, Studies of sorption of Th and Np on UO_2 and TiO_2, MRS Symp. Proc. 663 (2011) 1109–1115, doi:10.1557/PROC-663-1109.
[44] B. Torstenfelt, K. Andersson, B. Allard, Sorption of strontium and cesium on rocks and minerals, Chem. Geol. 36 (1982) 123–137, doi:10.1016/0009-2541(82)90042-0.
[45] D. Li, D.I. Kaplan, Sorption coefficients and molecular mechanisms of Pu, U, Np, Am and Tc to Fe (hydr)oxides: a review, J. Haz. Mater. 243 (2012) 1–18, doi:10.1016/j.jhazmat.2012.09.011.
[46] T. Missana, M.G. Gutiérrez, V. Fernńdez, Uranium (VI) sorption on colloidal magnetite under anoxic environment: experimental study and surface complexation modelling, Geochim. Cosmochim. Acta 67 (2003) 2543–2550, doi:10.1016/S0016-7037(02)01350-9.